

# Defect removal by solvent vapor annealing in thin films of lamellar diblock copolymers

Xinpeng Xu,<sup>1,2,\*</sup> Xingkun Man,<sup>3,4,†</sup> Masao Doi,<sup>3,4</sup> Zhong-can Ou-Yang,<sup>5</sup> and David Andelman<sup>6</sup>

<sup>1</sup>*Physics Program, Guangdong Technion – Israel Institute of Technology, Shantou, Guangdong Province 515063, P. R. China*

<sup>2</sup>*Faculty of Physics, Technion – Israel Institute of Technology, Haifa 32000, Israel*

<sup>3</sup>*Center of Soft Matter Physics and Its Applications, Beihang University, Beijing 100191, P. R. China*

<sup>4</sup>*School of Physics and Nuclear Energy Engineering, Beihang University, Beijing 100191, P. R. China*

<sup>5</sup>*CAS Key Laboratory of Theoretical Physics, Institute of Theoretical Physics, Chinese Academy of Sciences, Beijing 100190, China*

<sup>6</sup>*Raymond and Beverly Sackler School of Physics and Astronomy, Tel Aviv University, Ramat Aviv 69978, Tel Aviv, Israel*

(Dated: December 15, 2024)

Solvent vapor annealing (SVA) is known to be a simple, low-cost and highly efficient technique to produce defect-free diblock copolymer (BCP) thin films. Not only can the solvent dilute the BCP segmental interactions, but also it can vary the characteristic spacing of the BCP microstructures. We systematically investigate the effect of adding solvent into lamellar BCP thin films and its evaporation rate on the BCP defect removal. We find that the increase of the lamellar spacing as is induced by solvent removal facilitates more efficient removal of defects. The stability of a particular defect in a lamellar BCP thin film is given in terms of the swelling ratio and the solvent evaporation rate. Our results highlight the mechanisms of SVA in obtaining defect-free BCP thin films, as is desired in nanolithography and other industrial applications.

## 1. Introduction

Thin films of diblock copolymer (BCP) with extended and defect-free lateral order can serve as ideal templates or scaffolds for fabricating nanoscale functional materials, as is desired in nanolithography and ultrafiltration membrane applications [1, 2]. However, when a BCP thin film coats a solid substrate, it is usually kinetically trapped in a nonequilibrium and poorly ordered state with significant amount of defects, hindering the mainstream use of BCP thin films in nanotechnology. Further treatments are thus needed to facilitate the fabrication of defect-free microdomains. As examples to techniques that have been developed to tailor the self-assembly behavior of BCP thin films we mentioned electric field alignment [3, 4], shear alignment [5, 6], microwave annealing [7], and thermal annealing [1, 10–14]. Besides these approaches, solvent vapor annealing (SVA) [1, 2, 15–22] has been used to enhance the mobility of the polymer chains, and facilitates the annihilation of defects.

In a typical solvent vapor annealing process [1, 2, 15–22], the BCP thin film is first exposed to vapors of one or more solvents for certain amount of annealing time. After a swollen and mobile polymer film is formed on the substrate, then it is dried by controlled solvent evaporation. During the film swelling in SVA, solvent molecules diffuse into the thin BCP film and screen (or dilute) the unfavorable interactions between polymer segments, leading to a lower effective Flory-Huggins parameter,  $\chi_{\text{eff}}$ , than its value for dry (no solvent) case [23–25]. Note that  $\chi_{\text{eff}}(\phi_s)$

is a function of solvent volume fraction,  $\phi_s$ . In addition, as the polymer mobility is greatly enhanced with increasing  $\phi_s$ , the spacing  $\lambda$  of the microdomains also changes as a function  $\phi_s$  [2, 15–19, 26, 27].

Comparing to conventional thermal annealing (TA), SVA offers several unique advantages for defect annihilation [1, 2, 18]: (i) SVA provides means to anneal BCPs that are sensitive to thermal degradation. (ii) SVA is generally more effective (with shorter annealing time) in removing defects for thin films of high-molecular-weight BCPs. (iii) SVA provides additional controlling parameters for tuning film morphology. For example, solvent molecules allow the segregation  $\chi N$  to vary continuously (by varying the swelling ratio or the solvent volume fraction) over a larger range of values than what could be achieved in TA by just changing temperature. In addition, selective solvent can be used to induce asymmetric swelling between BCP blocks, and thus change the morphology of the BCP film.

Despite the widespread use of SVA, a quantitative understanding of its effects in defect removal has not yet been established [1, 2, 18, 22]. Two principal reasons are that no standardized SVA process has been established, and the connection between the nanostructure formed in the swollen film and the final dried film has not been rigorously formulated. Therefore, it is of interest to perform detailed studies on the effects of the relevant system parameters during the swelling and removal of solvent in SVA. Such parameters include swelling ratio, annealing time, solvent evaporation rates, film thickness, temperature, and solvent selectivity. The understanding of their effects on the morphology of BCP thin films is necessary to finely control the SVA process in order to obtain the

\* E-mail address: xu.xinpeng@gtit.edu.cn

† E-mail address: manxk@buaa.edu.cn

desired morphology.

Here, we propose a two-fluid model for SVA processes in BCP thin films, and carry out detailed numerical analysis on two of the major (dimensionless) system parameters: (i) Swelling ratio  $\mathcal{R}$ , representing the ratio of the swollen film volume  $V$  to its original volume  $V_0$ , i.e.,  $\mathcal{R} \equiv V/V_0$ . (ii) Normalized solvent evaporation rate  $\alpha_e \equiv \tau_e^{-1}/\tau_0^{-1}$  with  $\tau_e$  representing the characteristic time for complete evaporation of solvent in the swollen film and  $\tau_0$  characterizing the time for copolymer reorganization in the scale of microdomain period  $\lambda$ . To be specific, we investigate the removal of a typical defect occurring in symmetric BCP lamellae in their perpendicular orientation by SVA using non-selective solvent. Our main finding is that the increase in the lamellar spacing facilitates a more efficient removal of defects in BCP films. Moreover, the dependence of the final morphology of the dried BCP film on  $\mathcal{R}$  and  $\alpha_e$  is summarized in a stability diagram, which can be verified in future experiments.

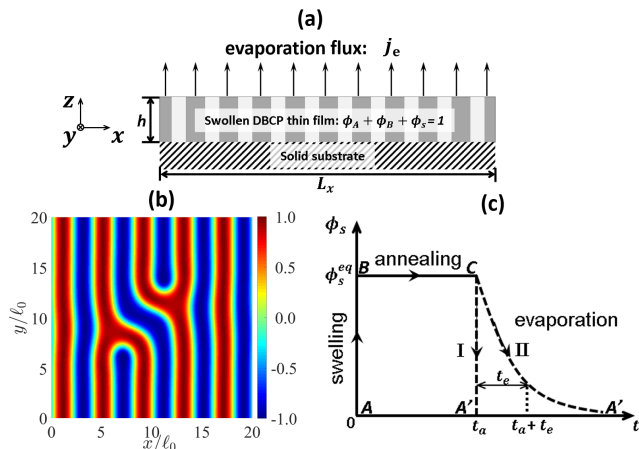


FIG. 1. (a) Schematic illustrations of the BCP film setup, (b) a snapshot of defect structure, and (c) a sketch of the temporal evolution of solvent volume fraction. Three important parameters are shown: the equilibrium solvent fraction of a swollen film  $\phi_s^{(eq)}$ , the annealing time  $\tau_a$ , and evaporation time  $\tau_e$ . In (c), the lines  $A \rightarrow B$ ,  $B \rightarrow C$  and  $C \rightarrow A'$  represent the subsequent swelling, annealing and evaporation processes, respectively.

## 2. Model Description and Numerical Method

### 2.1. Model

We consider a solution of monodisperse A/B diblock copolymers (BCP) dissolved in a non-selective good solvent for which the polymer-solvent interactions  $\chi_{AS} = \chi_{BS}$ . We restrict ourselves to symmetric A/B BCP where an A-block with  $N_A$  monomers is covalently bonded to a B-block with  $N_B$  monomers such that  $N_A = N_B = N/2$ ,

and  $N$  being the polymerization index. Furthermore, for simplicity, we assume incompressibility and zero volume change upon mixing in the BCP solution. Therefore, the chemical composition of BCP solutions is described by the solvent volume fraction  $\phi_S$  and an order parameter  $\phi \equiv \phi_A - \phi_B$  (the relative A/B volume fraction of the two blocks).

For non-selective solvent, we assume that the effective interaction parameter  $\chi_{\text{eff}}(\phi_S)$  satisfies [23–25]

$$\chi_{\text{eff}} = \chi(\phi_P)^\delta = \chi(1 - \phi_S)^\delta, \quad (1)$$

with  $\delta$  varying from 1.0 to 1.6 over a large range of  $\phi_S$  values [23–25]. Adding a non-selective solvent in BCP melt has a similar effect on the BCP melt microstructure as increasing the temperature [18, 19]. Namely, it shifts the BCP coexisting phases towards higher temperatures in the temperature-composition plane [31].

Yet the solvent has an additional effect where it changes the spacing of BCP lamellae that can be approximated by a power law [16]

$$\lambda = \lambda_0(1 - \phi_S)^{-\beta}, \quad (2)$$

where  $\lambda_0$  is the lamellar spacing in a dry BCP film ( $\phi_S = 0$ ) and  $\beta$  (positive or negative) is a material parameter that depends on the degree of solvent selectivity, solvent volume fraction, and morphology of the ordered state. For example, it was found experimentally that  $\beta \approx -0.3$  in dense BCP solutions of PS-PI with nonselective solvents (at small solvent volume fraction) [26, 27].

In our present work, we will consider BCP solutions with nonselective solvent as being equivalently to BCP melts with an effective  $\chi_{\text{eff}}$  parameter and microdomain spacing  $\lambda$ . The former can be described by the same Landau-Brazovskii free-energy as was modeled in the past for BCP melts (See Supporting Information for details) but with

$$\tau \simeq 2\rho_c N(\chi_c - \chi_{\text{eff}}), \quad q \equiv (1 - \phi_S)^\beta q_0, \quad (3)$$

with  $\rho_c$  being the copolymer closed packing chain density of the melts, and  $q_0 = 2\pi/\lambda_0$  and  $q = 2\pi/\lambda$  being the  $q$ -wavenumber of the dry and swollen states, respectively.

With such a modified free-energy, we formulate a two-fluid model for the BCP solutions with non-selective solvent to explore the dynamic coupling between BCP copolymers and small solvent molecules during SVA (See Supporting Information for details). This is in analogy to a two-fluid model used to model polymer solutions, polymer blends, and diblock copolymer melts [32–37].

We consider the limit of no macroscopic convection [33, 34] and focus on thin films of concentrated BCP solutions (with relatively small  $\phi_S$ ) where the relaxation dynamics throughout the film thickness ( $z$ -direction) is much faster than the lateral ( $xy$ -plane) dynamics (as schematically shown in Fig. 1a). This limit is justified when the viscous time scale  $\tau_v = h^2/\nu$  (with  $\nu$  being the kinematic viscosity of the BCP solution) is much smaller than the

evaporative time  $\tau_e = h_0/v_e$  for an initially stationary film to evaporate to dry film, i.e.,  $\tau_v \ll \tau_e$ . Furthermore, we focus on the simple case that the evaporation of solvent is *slow* relative to vertical solvent/polymer diffusion, i.e.,  $\tau_e \gg \tau_S, \tau_P$  with  $\tau_S = h_0^2/D_S$  and  $\tau_P = h_0^2/D_P$  being the diffusion times through the film thickness of the solvent and the polymer segments, respectively, and  $D_S$  and  $D_P$  the corresponding collective diffusion constants. In this case, the variations of phase structure, measured by  $\phi$ , and solvent distribution  $\phi_S$  are negligible in the normal ( $z$ -) direction, yielding  $\phi = \phi(x, y, t)$  and  $\phi_S = \phi_S(t)$ .

Under such assumptions, the evolution of the film thickness, the integrated solvent fraction, and the phase structure of BCP thin film is written as

$$h = h_0/(1 - \phi_S), \quad (4)$$

$$\partial_t \phi_S = -\tau_e^{-1}(1 - \phi_S)^2(\phi_S - \phi_S^{(\text{eq})}), \quad (5)$$

$$\partial_t \phi = \nabla_{\parallel} \cdot (M_{\phi\phi} \nabla_{\parallel} \mu_{\phi}). \quad (6)$$

where  $M_{\phi\phi}$  is the mobility coefficient, and  $\mu_{\phi}$  is the chemical potential of the BCP solution.

## 2.2. Numerical Method and System Setup

Using the classical central finite-difference method [35, 43], we numerically integrate the dynamical equation (6) for the order parameter  $\phi$ , and eq. (5) for the solvent fraction  $\phi_S$  (in the  $xy$ -plane), as is schematically shown in Fig. 1a. The mesh size of our simulation box is chosen to be  $\ell_0 \approx 0.25\lambda_0$ . The simulation box size is taken to be  $L_x = L_y = 20\ell_0$ . Periodic boundary conditions are employed in both directions. Time is measured in units of

$$\tau_0 \equiv \ell_0^2/\rho_c M_{\phi\phi}, \quad (7)$$

which characterizes the time for copolymer reorganization in the scale of microdomain period  $\lambda_0 \sim \ell_0$ . Note that the number of lamellar periods equals to an integer that is the closest to  $L_x/\lambda_0$ . It is *five* for  $L_x = 20\ell_0$  and dry lamellar spacing  $\lambda_0 \approx 4.0\ell_0$ , as can be seen in Fig. 1b.

We carry out a numerical study for the effects of solvent swelling and solvent evaporation on the morphology of a dry BCP film with a particular defect as shown in Fig. 1b. The uptake (swelling) rate of solvent usually strongly depends on the morphology of BCP film even for a non-selective solvent [16]. However, in experiments the exposure time to solvent vapor (the annealing time) is usually longer than that required for the film to swell and reach an equilibrium (solvent) volume fraction [16, 18]. In our simulations, we ignore the effects of solvent uptake process and assume “instantaneous” saturation to equilibrium (solvent) volume fraction  $\phi_S^{(\text{eq})}$  as schematically shown in Fig. 1c. After an annealing time  $\tau_a$ , the solvent is removed by a controlled evaporation rate,  $\tau_e^{-1}$ , according to eq. (5).

## 3. Results and Discussion

We present results about the effects of two key pa-

rameters on the defect removal during SVA: solvent-swelling ratio  $\mathcal{R}$ , that is a monotonic function of equilibrium volume fraction  $\phi_S^{(\text{eq})}$ , and the normalized solvent-evaporation rate,  $\alpha_e = \tau_e^{-1}/\tau_0^{-1}$ .

### 3.1. Effects of solvent-swelling ratio

The swelling of the film is one-dimensional along the normal  $z$ -direction of the film, due to the lateral confinement of fixed area set by periodic boundary conditions, as shown in Fig. 1a. The swelling ratio  $\mathcal{R} \equiv V/V_0$  is then given by

$$\mathcal{R} = h/h_0 = (1 - \phi_S^{(\text{eq})})^{-1} \quad (8)$$

from the conservation of copolymers and eq. (4) with  $h_0$  and  $h$  being the film thicknesses of the original dry film and the swollen film, respectively.

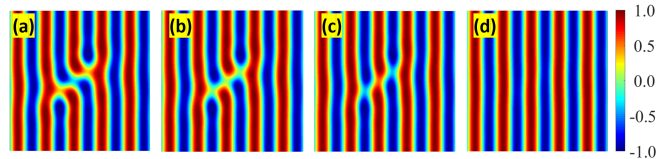


FIG. 2. Defect removal upon instantaneous solvent swelling due to the dilution effects only on  $\chi_{\text{eff}}$  as given in eq. (1),  $\chi(1 - \phi_S)$ . Here the equilibrium solvent volume fraction  $\phi_S^{(\text{eq})}$  is taken to be 0.6, corresponding to swelling ratio  $\mathcal{R} = 2.5$ .

As pointed out in the previous section, there are two major effects of a non-selective solvent in a swollen BCP film: diluting effect on  $\chi_{\text{eff}}(\phi_S)$ , eq. (1), and changing the lamellar spacing  $\lambda(\phi_S)$ , eq. (2). We first carry out simulations to study a simple case when the changes in lamellar spacing are negligible during solvent annealing. The results show that the defect stability strongly depends on the solvent fraction  $\phi_S^{(\text{eq})}$  (or swelling ratio  $\mathcal{R}$  given in Eq. (8)) in the swollen film.

For a relatively low swelling ratio  $\mathcal{R}$  (small  $\phi_S^{(\text{eq})}$ ), the system is kinetically trapped (metastable). In the other limit of very large swelling ratio when  $\chi_{\text{eff}} < \chi_c$  (equivalently,  $\mathcal{R} > 2.86$  or  $\phi_S^{(\text{eq})} > 0.65$ ), the BCP undergoes an order-disorder transition (ODT), and the BCP solutions evolve to a disordered state without microphase separated structure. As shown in Fig. 2, only in a limited range of swelling ratio,  $2.5 < \mathcal{R} < 2.86$  (or equivalently  $0.6 < \phi_S^{(\text{eq})} < 0.65$ ), the copolymer segments gain large enough mobility but still maintain an ordered structure such that the defect-free lamellar structure is obtained.

The mechanism of defect removal by adding solvent to reduce  $\chi$  is very similar to a thermal annealing (TA) by increasing temperature also reducing  $\chi \sim 1/T$  [10–12]. However, it is interesting to note that the kinetic pathway during the defect removal using SVA is quite different from the one using TA. For TA, the defect removal pathway is asymmetric [11] in the sense that the two horizontal arms in the defect shown in Fig. 1b break

sequentially, one by one. In contrast, for SVA, the defect removal pathway is symmetric in the sense that the two horizontal arms break simultaneously, as seen in Fig. 2a.

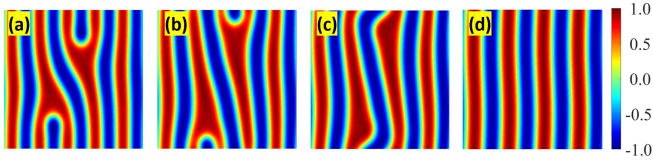


FIG. 3. Destabilization of defects upon instantaneous solvent swelling due to an increase in the lamellar spacing. Here, we take  $\phi_S^{(\text{eq})} = 0.4$  (corresponding to  $\mathcal{R} \approx 1.67$ ) and  $\beta = 1.0$  as defined in Eq. (2). In this case, the energy-preferred number of lamellar periods changes from five (at dry state) to three (at swollen state).

More generally, the change in lamellar spacing  $\lambda$  during solvent annealing of BCP films is visible and cannot be neglected [2, 18, 19]. At small  $\phi_S^{(\text{eq})}$  below some critical value [26, 27], the spacing  $\lambda$  increases with increasing solvent volume fraction. In Fig. 3 we take  $\phi_S^{(\text{eq})} = 0.4$  and the equilibrium lamellar spacing increases from  $\lambda_0 \approx 4\ell_0$  for the dry state to  $\lambda \approx 6\ell_0$  for the swollen state. Correspondingly, the energy-preferred number of lamellar periods changes from five to three. Fig. 3 shows that such an increase in lamellar spacing tends to drive long-wavelength structural evolution. Note that after defect removal the system evolves to a metastable defect-free state with four lamellar periods instead of energy-preferred three periods. This again indicates the addition of solvent alters the kinetic pathway of the microstructure evolution of the BCP film.

In addition, comparing these results with spacing changes to those without spacing changes (for example, results shown in Fig. 2), we find that for  $\phi_S^{(\text{eq})} = 0.4$ , the defect structure is still metastable in the latter case without spacing changes, but becomes unstable in the former case with spacing changes (as shown in Fig. 3). We conclude that the solvent-induced increase in lamellar spacing facilitates a more efficient removal of defects.

### 3.2. Effects of solvent-evaporation rate

It is well-known that the final morphology of the dried BCP film depends, not only on the swelling ratio  $\mathcal{R}$  and the morphology in the swollen state, but also on the evaporation rate of solvent,  $\alpha_e$  [2, 16, 18, 19]. To examine this dependence, we carry out simulations for swollen films with different swelling ratio  $\mathcal{R}$  (i.e., with different  $\phi_S^{(\text{eq})}$ ) and for solvent evaporation at different rates  $\alpha_e$ . As schematically shown in Fig. 1c, the solvent is removed by evaporation following eq. (5) after time  $\tau_a$  of solvent annealing.

For small swelling ratio  $\mathcal{R} < 1.2$  (i.e.,  $\phi_S^{(\text{eq})} < 0.15$ ), the amount of solvent in the swollen film is not sufficient to enhance polymer chain mobility such that the original defect is still metastable and kinetically trapped. In the

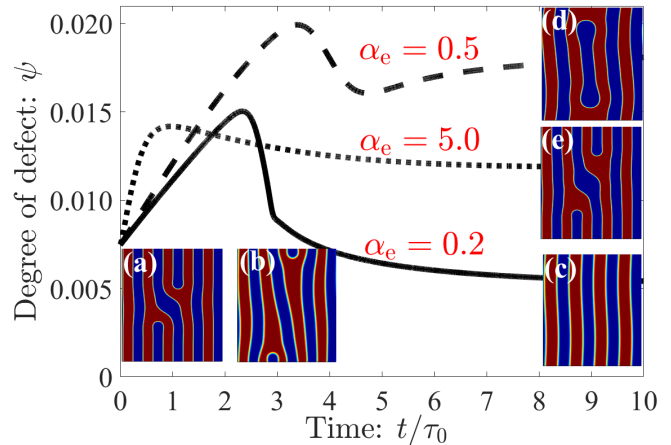


FIG. 4. The temporal evolution of the defect structure (shown in Fig. 1b) of a swollen BCP film at various evaporation rates  $\alpha_e$  after annealing time  $\tau_a = 0.48\tau_0$  at solvent fraction  $\phi_S^{(\text{eq})} = 0.4$ . The degree of defect is defined by  $\psi \equiv \sum_{i,j} (\phi_{i,j} - \phi_{i,1})^2$  (with  $i, j$  denoting the sites in the computational box) to quantify the process of defect removal. (Inset) Snapshots of the temporal evolution of the original defect (a) (no solvent) upon different evaporation rates  $\alpha_e$ . For slow evaporation, the defect (a) is removed spontaneously to a defect-free state (c) after crossing a transition state (b). In contrast, for faster evaporation, the defect (a) is either kinetically trapped as in (e) or unstable and re-trapped to a new defect state (d).

dried film after solvent evaporation, the original defect persists and is found to be independent of the evaporation rate.

In contrast, at large swelling ratio  $\mathcal{R} > 2.86$  (i.e.,  $\phi_S^{(\text{eq})} > 0.65$ ) where  $\chi_{\text{eff}}N < \chi_c N$ , the system passes through the ODT and the swollen BCP film is disordered. After the solvent evaporates, the film re-enters the ordered phase but the final dry film is usually trapped in a poorly ordered state with significant amount of defects and the detailed phase structures strongly depend on the evaporation rates. To obtain a defect-free state, one has to direct the film morphology by well controlling the solvent evaporation rate [39, 40, 44], or applying shear flows [5, 6].

At intermediate swelling ratio  $\mathcal{R} \sim 1.7$  (i.e.,  $\phi_S^{(\text{eq})} \sim 0.4$ ), the copolymer chains have sufficient mobility and the defect is removed spontaneously if the annealing time  $\tau_a$  is large enough, as shown in Fig. 3. In SVA experiments, the solvent is usually evaporated after some small annealing time. In our simulations, the solvent evaporates after an annealing time  $\tau_a = 0.48\tau_0$ . We find that the phase structure of the dried film strongly depends on the evaporation rate  $\alpha_e = \tau_e^{-1}/\tau_0^{-1}$  as shown in Fig. 4. The initial defect Fig. 4a can be removed only at slow evaporation with  $\alpha_e \ll 1$  in Fig. 4c (a snapshot before the defect is removed is also shown in Fig. 4b). At fast evaporation,  $\alpha_e \gg 1$ , the defect persists as shown in Fig. 4e, while at intermediate evaporation rates with

$\alpha_e \sim 1$ , the initial defect becomes unstable but is re-trapped to another defective structure (but with larger spacing) as shown in Fig. 4d.

All these results can be understood in terms of the evaporation time  $\tau_e$ , which allows the copolymers to reorganize during the solvent removal process (with characteristic time  $\tau_0$ ). On the other hand, when the solvent is removed rapidly, the copolymers lose mobility almost instantly, and are kinetically trapped into the defective swollen morphology. When the solvent is removed gradually, the domain spacing changes and the defects are destabilized; moreover the BCP microdomains have time to relax such that the defects can be removed just as in the case of very long annealing times (without solvent evaporation). In the annealing process of thin BCP films on neutral substrates by non-selective solvents, the most efficient pathway to remove defects is first to swell the film to a sufficiently large solvent fraction where defects become unstable, and only then to evaporate the solvent rapidly when the defect is almost “healed” spontaneously.

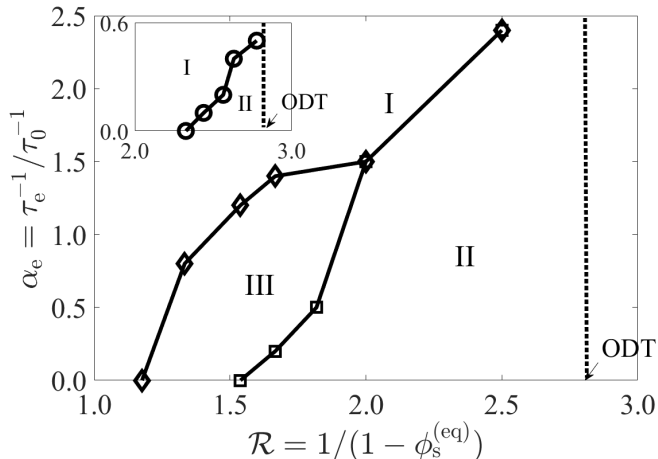


FIG. 5. Stability diagram of the defect shown in Fig. 1b during SVA due to the dilution effects and the changes in lamellar spacing. The diagram is plotted in terms of two parameters: the swelling ratio  $\mathcal{R} = 1/(1 - \phi_s^{(eq)})$  and the evaporation rate  $\alpha_e = \tau_e^{-1}/\tau_0^{-1}$ . Three regions are identified: (I). *Stable-defect region* – the original defect is still (meta-) stable. (II). *Defect-free region* – the defect becomes unstable and is removed spontaneously. (III). *Intermediate-defect region* – the original defect is unstable but is re-trapped to a new defect state. The lines are shown to guide the eyes. (Inset) Stability diagram of the defect in the case without spacing changes during SVA.

In addition, we note that the dependence of the final morphology of dried BCP films on solvent-swelling ratio  $\mathcal{R}$  and solvent-evaporation rate  $\alpha_e$  can be summarized in a stability diagram of the defect as shown in Fig. 5. Three regions are identified: (I). Stable-defect region at small  $\mathcal{R}$  and large  $\alpha_e$ , in which the original defect is still stable or metastable and persists in the dried film. (II). Defect-free region at large  $\mathcal{R}$  and small  $\alpha_e$ , in which the defect

becomes unstable and is removed spontaneously. (III). Intermediate-defect region, in which the original defect is unstable but is re-trapped in a new defect state. When the solvent-induced changes in lamellar spacing are negligible (see the inset of Fig. 5). There are only two regions: (I). Stable-defect region, and (II). Defect-free region; the intermediate-defect region (III) does not appear. Moreover, the defect-free region (II) is much smaller when the spacing changes. Such a stability diagram should be verified in future experiments.

Finally, we would like to point out that at large solvent fraction (over some crossover value  $\phi_s^*$ ), the addition of solvent can induce decrease of lamellar spacing in both bulk BCP solutions [26, 27] and BCP films [2, 18, 19]. For example,  $\phi_s^* \approx 0.3$  for polystyrene-polyisoprene (PS-PI) copolymer in solutions with non-selective solvent [26]). To explore the effects of solvent induced decrease in lamellar spacing, we have also carried out more simulations (See Supporting Information for details). We find that the solvent-induced spacing decreases at large  $\phi_s$  induces small-wavelength undulations in contrast to the long wavelength structural evolution, as shown in Fig. 3. These small-wavelength undulations are usually not enough to remove defects. Efficient defect removal occurs only for cases with significant spacing-increase during solvent annealing at small solvent fraction (when  $\phi_s < \phi_s^*$ ).

## 4. Conclusions

In summary, we have constructed a two-fluid model to study the microphase separation dynamics of block copolymer (BCP) thin films and applied it to solvent vapor annealing (SVA) processes. We focus on the effects of added (non-selective) solvent on the defect annihilation in ordered BCP thin films on neutral substrates. More specifically, we investigate the solvent-facilitated removal of a typical defect occurring in symmetric lamellar BCP thin films with perpendicular (to the substrate) lamellae.

One of our key findings is that the added solvent not only dilutes the unfavorable interactions between polymer segments, but also changes the characteristic spacing of the BCP lamellae. We find that the solvent-induced increase of the lamellar spacing in dense polymer solution (that is at small solvent volume fraction) facilitates an efficient removal of defects. The kinetic pathways of defect removal during SVA are quite different from that of thermal annealing (TA) and show sensitive dependence on the volume fraction and dynamics of added solvent. The final morphology of the dried BCP film after SVA depend not only on solvent-swelling ratio  $\mathcal{R}$  (or solvent volume fraction) but also solvent-evaporation rate  $\alpha_e$ . Such a dependence is summarized in a stability diagram (Fig. 5), which can be verified in future experiments.

Based on these results, we are able to make an important observation about the annealing of thin BCP films on neutral substrates by non-selective solvents. Namely, the most efficient pathway to remove the defects is to first swell the film to a sufficiently large solvent fraction where defects become unstable, and only then to evapo-

rate the solvent rapidly when the defect almost “heals” spontaneously. We believe that the insight provided in this theoretical work on defect removal from perpendicular lamellar BCP thin films by SVA has the potential to greatly expand and diversify the range of applications of solvent-assisted, directed self-assembly of BCP thin films.

## Acknowledgments

We would like to thank S. Komura and T. Qian for discussions and helpful suggestions. This work was supported in part by Grant No. 21822302 and 21434001 of the National Natural Science Foundation of China (NSFC), the joint NSFC-ISF Research Program, jointly funded by the NSFC under Grant No. 51561145002 and the Israel Sci-

ence Foundation (ISF) under Grant No. 885/15. X. X. was supported by Guangdong Technion – Israel Institute of Technology. D.A. acknowledges the hospitality of the ITP (CAS) and Beihang University, Beijing, China, and a CAS President International Fellowship Initiative (PIFI).

## Conflict of Interest

The authors declare no conflict of interest.

## Keywords

block copolymer, solvent vapor annealing, defect removal, two-fluid model, Onsager’s variational principle

- 
- [1] J. N. Albert, T. H. Epps III, *Mater. Today* **2010**, 13, 24.
- [2] C. Sinturel, M. Vayer, M. Morris, M. A. Hillmyer, *Macromolecules* **2013**, 46, 5399.
- [3] T. Morkved, M. Lu, A. Urbas, E. Ehrichs, H. Jaeger, P. Mansky, T. Russell, *Science* **1996**, 273, 931.
- [4] T. Thurn-Albrecht, J. Schotter, G. Kästle, N. Emley, T. Shibauchi, L. Krusin-Elbaum, K. Guarini, C. Black, M. Tuominen, T. Russell, *Science* **2000**, 290, 2126.
- [5] A. P. Marencic, M. W. Wu, R. A. Register, P. M. Chaikin, *Macromolecules* **2007**, 40, 7299.
- [6] C. K. Shelton, R. L. Jones, T. H. Epps III, *Macromolecules* **2017**, 50, 5367.
- [7] X. Zhang, K. D. Harris, N. L. Wu, J. N. Murphy, and J. M. Buriak, *ACS Nano* **2010**, 4, 7021.
- [8] T. Kubo, J. Parker, M. Hillmyer, and C. Leighton, *Appl. Phys. Lett.* **2007**, 90, 233113.
- [9] T. Kubo, R. Wang, D. Olson, M. Rodwogin, M. Hillmyer, and C. Leighton, *Appl. Phys. Lett.* **2008**, 93, 133112.
- [10] W. Li, M. Müller, *Annu. Rev. Chem. Biomol. Eng.* **2015**, 6, 187.
- [11] W. Li, P. F. Nealey, J. J. de Pablo, M. Müller, *Phys. Rev. Lett.* **2014**, 113, 168301.
- [12] S.-M. Hur, V. Thapar, A. Ramírez-Hernández, G. Khaira, T. Segal-Peretz, P. A. Rincon-Delgadillo, W. Li, M. Müller, P. F. Nealey, and J. J. de Pablo, *Proc. Natl. Acad. Sci.* **2015**, 112, 14144.
- [13] X. K. Man, D. Andelman, and H. Orland, *Phys. Rev. E* **2012**, 010801.
- [14] X. K. Man, P. Zhou, J. Tang, D. Yan, and D. Andelman, *Macromolecules* **2016**, 49, 8241.
- [15] Jianqi Zhang, Dorthe Posselt, Alessandro Sepe, Xuhu Shen, Jan Perlich, Detlef-M. Smilgies, Christine M. Papadakis, *Macromol. Rapid Commun.* **2013**, 34, 1289.
- [16] J. Zhang, D. Posselt, D.-M. Smilgies, J. Perlich, K. Kyriakos, S. Jaksch, C. M. Papadakis, *Macromolecules* **2014**, 47, 5711.
- [17] Andrey A. Rudov, Elena S. Patyukova, Irina V. Neratova, Pavel G. Khalatur, Dorthe Posselt, Christine M. Papadakis, Igor I. Potemkin, *Macromolecules* **2013**, 46, 5786.
- [18] X. Gu, *Self-assembly of block copolymers by solvent vapor annealing, mechanism and litho graphic applications*, Ph.D. thesis, University of Massachusetts Amherst **2014**.
- [19] X. Gu, I. Gunkel, A. Hexemer, T. Russell, *Macromolecules* **2016**, 49, 3373.
- [20] G. Kim, M. Libera, *Macromolecules* **1998**, 31, 2569.
- [21] K. A. Cavicchi, T. P. Russell, *Macromolecules* **1996**, 40, 1181.
- [22] J. Hao, Z. Wang, Z. Wang, Y. Yin, R. Jiang, B. Li, Q. Wang, *Macromolecules* **2017**, 50, 4384.
- [23] E. Helfand, Y. Tagami, *J. Chem. Phys.* **1972**, 56, 3592.
- [24] T. Lodge, C. Pan, X. Jin, Z. Liu, J. Zhao, W. Maurer, F. Bates, *J. Polym. Sci. B* **1995**, 33, 2289.
- [25] J. Naughton, M. W. Matsen, *Macromolecules* **2002**, 35, 5688.
- [26] M. Shibayama, T. Hashimoto, H. Hasegawa, H. Kawai, *Macromolecules* **1983**, 16, 1427.
- [27] M. Shibayama, T. Hashimoto, H. Kawai, *Macromolecules* **1983**, 16, 1434.
- [28] Roland R. Netz, David Andelman, M. Schick, *Phys. Rev. Lett.* **1997**, 79, 1058.
- [29] Y. Tsori, D. Andelman, *Macromolecules* **2002**, 35, 5161.
- [30] A. Ciach, J. Pekalski, W. Gozdz, *Soft Matter* **2013**, 9, 6301.
- [31] C.-I. Huang, T. P. Lodge, *Macromolecules* **1998**, 31, 3556.
- [32] A. Onuki, *J. Phys. Soc. Jpn.* **1990**, 59, 3427.
- [33] M. Doi, A. Onuki, *Journal de Physique II* **1992**, 2, 1631.
- [34] S. T. Milner, *Phys. Rev. E* **1993**, 48, 3674.
- [35] G. Buxton, N. Clarke, *EPL* **2007**, 78, 56006.
- [36] C.-D. Yoo, J. Viñals, *Macromolecules* **2012**, 45, 4848.
- [37] S. Yabunaka, T. Ohta, N. Yoshinaga, *J. Chem. Phys.* **2012**, 136, 074904.
- [38] X. Xu, U. Thiele, T. Qian, *J. Phys. Condens. Matter* **2015**, 27, 085005.
- [39] S. P. Paradiso, K. T. Delaney, C. J. García-Cervera, H. D. Ceniceros, G. H. Fredrickson, *ACS Macro Letters* **2013**, 3, 16.
- [40] S. P. Paradiso, K. T. Delaney, C. J. García-Cervera, H. D. Ceniceros, G. H. Fredrickson, *Macromolecules* **2016**, 49, 1743.
- [41] F. Liu, N. Goldenfeld, *Phys. Rev. A* **1989**, 39, 4805.
- [42] M. Müller, W. Li, J. C. O. Rey, U. Welling, *J. Phys. Conf. Ser.* **2015**, 640, 012010.
- [43] S. C. Glotzer, *Annu. Rev. Comput. Phys.* **1995**, 2, 1.
- [44] J. N. Albert, W.-S. Young, R. L. Lewis III, T. D. Bogart, J. R. Smith, T. H. Epps III, *ACS Nano* **2011**, 6, 459.